IEEE Access
Multidisciplinary | Rapid Review | Open Access Journal

Received 30 November 2023, accepted 13 January 2024, date of publication 17 January 2024, date of current version 24 January 2024.

Digital Object Identifier 10.1109/ACCESS.2024.3355145

RESEARCH ARTICLE

Machine Learning-Optimized Compact Frequency Reconfigurable Antenna With RSSI Enhancement for Long-Range Applications

MUHAMMAD S. YAHYA[1,4], (Graduate Student Member, IEEE), SOCHEATRA SOEUNG[1], (Senior Member, IEEE), SHARUL KAMAL ABDUL RAHIM[2], (Senior Member, IEEE), UMAR MUSA[3], (Graduate Student Member, IEEE), SAEED S. BA HASHWAN[5], AND MD. ASHRAFUL HAQUE[1,6], (Graduate Student Member, IEEE)

[1]Department of Electrical and Electronic Engineering, Universiti Teknologi PETRONAS, Seri Iskandar, Perak 32610, Malaysia
[2]Wireless Communication Centre, Universiti Teknologi Malaysia, Skudai, Johor 81310, Malaysia
[3]Faculty of Electrical and Electronic Engineering, University Tun Hussein Onn, Parit Raja, Johor 86400, Malaysia
[4]Department of Electrical and Electronic Engineering, Abubakar Tafawa Balewa University, Bauchi 740272, Nigeria
[5]Department of Electronics Communication Engineering, Faculty of Engineering Petroleum, Hadhramout University, Al Mukalla, Hadhramout, Yemen
[6]Department of Electrical and Electronic Engineering, Daffodil International University, Dhaka 1341, Bangladesh

Corresponding authors: Socheatra Soeung (socheatra.s@utp.edu.my) and Saeed S. Ba Hashwan (saeedsb2013@gmail.com)

This work was supported in part by Universiti Teknologi PETRONAS, Malaysia, YUTP-PRG (Yayasan Universiti Teknologi PETRONAS-Prototype Research Grant) under Grant (015PBC-007); in part by the Ministry of Higher Education Malaysia; and in part by Universiti Teknologi Malaysia under Grant 4J611, Grant 4B536, Grant 4B888, Grant 03M81, Grant 04M36, and Grant 4C599.

ABSTRACT This study presents an innovative and compact monopole antenna with dual-band frequency reconfigurability for LoRa applications. It operates within the 915 MHz and 868 MHz frequencies, aligning with the designated bands for use in America, Asia and Europe. No existing compact reconfigurable antenna with these features for LoRa applications within ISM bands below 1 GHz is known. Employing an economical FR-4 substrate in its design, the antenna attains a compact size of 40 × 42 mm^2 (0.12 λ_0 × 0.12 λ_0), where λ_0 denotes the wavelength in free space corresponding to 868 MHz. A single RF PIN diode enables seamless switching between 868 MHz and 915 MHz bands. Design, simulation, and optimization employed CST MWS® software. Supervised regression Machine Learning (ML) models predicted resonance frequencies, with Gaussian Process Regression emerging as optimal, achieving R-squared and variance scores of 92.87% and 93.77%, respectively. A maximum gain of 2 dBi at 915 MHz and 70% efficiency, boasting good radiation patterns and matching was demonstrated by the antenna. Experimental validation in a football field at Universiti Teknologi PETRONAS, Malaysia, assessed the proposed antenna's performance on a LoRa transceiver system based on LoRa SX1276. The Received Signal Strength Indicator (RSSI) of the proposed antenna consistently exceeded the conventional commercially available monopole antenna by an average of −12 dBm at every point up to 300 m, showcasing enhanced signal reception. The antenna proves promising for wireless sensor nodes in long-range applications.

INDEX TERMS Dual-band, LoRa, PIN-diode, reconfigurable, RSSI.

I. INTRODUCTION

In our contemporary lives, the Internet of Things (IoT) stands as a transformative force, seamlessly connecting diverse objects to a central network and facilitating information exchange. This powerful and omnipresent technology enables individuals to remotely manage or monitor objects from systems located hundreds of kilometers away, employing diverse IoT technologies [1]. In the context of the fourth industrial revolution, the IoT emerges as a pivotal force,

The associate editor coordinating the review of this manuscript and approving it for publication was Yi Ren.

poised to shape the future with billions, if not trillions, of interconnected devices. Its exponential growth is foreseen to be a cornerstone of the evolving technological landscape, particularly as [2] predicts a connection of over 75 billion devices to the Internet by 2025.

IoT has revolutionized daily life by seamlessly connecting ordinary objects, transforming them into smart devices that bridge the physical and digital worlds [3]. This transformative power extends beyond personal convenience to impact diverse industries, offering innovative solutions that enhance both professional and personal domains.

In the era of smart devices, there is a growing demand for communication technologies with reliable long-range connectivity, low-cost, and power-efficient solutions [4]. Addressing this need, LPWANs (Low Power Wide Area Networks) have surfaced as a crucial solution, offering a scalable, power-efficient, and long-range communication platform for IoT applications [5], [6].

The foundation of LPWANs often relies on technologies like LoRa (Long Range), wherein the physical layer is served by LoRa radio and and the MAC layer is operated by Long Range Wide Area Networks (LoRaWAN). LoRaWAN adopts a star topology, facilitating communication between the Network Gateway (GW) and multiple End Devices (EDs). To ensure reliable long-range communication, CSS (Chirp Spread Spectrum) modulation is employed to effectively manage interference in LoRa signals. Moreover, the Adaptive Data Rate (ADR) mechanism enables dynamic adjustment of critical LoRa parameters—like carrier frequency, Spreading Factor (SF), Code Rate (CR), and Spreading Factor (SF)—allowing adaptation to varying communication conditions in dense networks [2], [7].

In addition to its technological attributes, the efficacy of LoRa communication is closely tied to the performance of antennas. In wireless communication systems domain, the critical role of antennas is evident as they facilitate both the transmission and reception of signals [8], [9], [10], with LoRa being no exception. The choice of antennas in LoRa technology significantly influences the range, coverage, and overall reliability of IoT applications. Proper antenna design ensures optimal signal propagation, allowing for extended communication distances and improved connectivity in diverse environments.

The surge in internet-connected devices highlights the need for compact and versatile wireless solutions. Reconfigurable antennas, especially small and lightweight ones like patch antennas, play a key role in meeting this demand. As technology evolves, the growing demand is for devices capable of multitasking. The emergence of IoT and the Industrial Internet of Things (IIoT) emphasizes the importance of wireless systems adaptable to various tasks, underscoring the significance of antennas with reconfigurable properties. A compact antenna with the ability to adjust frequency as needed becomes crucial for enhancing device functionality [11].

In the preceding decade, notable strides have been taken in the conceptualization and realization of antennas specifically designed for LoRa applications. Researchers have systematically explored a variety of antenna types, materials, and configurations, all directed towards optimizing the performance of LoRa antenna for IoT systems.

In [12], an antenna aimed for 923 MHz LoRa IoT applications was designed and fabricated. The antenna utilized folded monopole techniques and adopted an inverted-F configuration to achieve compactness and size reduction. The fabrication of the antenna having a dimension of $13.11 \times 22.95\ \text{mm}^2$ was implemented on FR-4 PCB material. Despite its low profile, the antenna demonstrated -11.86 dBi as its maximum gain at the designed frequency, and it featured an omnidirectional radiation pattern, ensuring efficient signal propagation in all directions. However, the antenna's fixed frequency design and relatively low gain raise considerations about its suitability for IoT applications, especially in scenarios requiring higher gain or frequency agility.

In a study by [13], a compact antenna designed for LoRa sensor node IoT applications was discussed. Fabricated on an FR-4 substrate utilizing a PIFA structure, the antenna seamlessly integrated cut slots on its ground plane, resulting in a deliberate reduction of the operating frequency to 410 MHz from 450 MHz. Strategically positioned at the edge of a compact LoRa sensor node circuit board measuring 125 mm $\times$ 103 mm $\times$ 1.6, mm, the antenna effectively occupied a space measuring 125 mm $\times$ 20 mm $\times$ 1.6 mm. Operating effectively between 402.4 MHz and 441.6 MHz with $S_{11} < -6\,\text{dB}$, the antenna showcased a nearly omnidirectional radiation pattern. However, challenges were noted, including a lower realized gain (-6 dBi) and relatively larger dimensions. Furthermore, the fixed-frequency design may present difficulties in scenarios requiring frequency adaptability for diverse IoT applications.

Additionally, a method for downsizing a patch antenna to operate below 1 GHz for LoRa applications was presented in [14]. The study introduced a rectangular patch antenna featuring an inset feed which was initially designed at 1.57 GHz on an FR-4 substrate using Ansys HFSS. A slot was incorporated just below the patch to shift the resonance frequency to 881 MHz. The evaluated $S_{11} < -10\,dB$ characteristic of the antenna revealed that the fabricated antenna achieved a gain of 0.58 dB. However, it is noteworthy that the gain remains relatively low, and the fixed frequency design may pose limitations in scenarios requiring flexibility for various IoT applications.

A comprehensive investigation by [15] explored the development of a multiband MPA on an FR-4 PCB material. Featuring a rectangular patch with strategically positioned slots, the antenna aimed for multiband functionality, covering LoRaWAN, UMTS, and European GSM-1800 frequency bands for RF energy harvesting. It's noteworthy that despite its multiband capability, the antenna lacks reconfigurability and is limited to a single LoRa band, potentially constraining

its adaptability to diverse frequency requirements in the LoRa spectrum.

In the pursuit of miniaturizing antennas for LoRaWAN applications, a microstrip meandered line was introduced to induce a lower resonance in the PIFA structure [16]. This involved incorporating a meandered microstrip line on an FR-4 substrate, extending the current path and resulting in a downward shift of the antenna's resonant frequency. While this technique proved effective for achieving compact antenna designs, it is essential to note its limitation in terms of fixed frequency operation (non-reconfigurable). The optimized antenna, measuring $40 \times 26 \times 1.6$ mm^3, exhibited a bandwidth of 102 MHz, ranging from 848 MHz to 950 MHz, and a maximum gain of 2.1 dBi across its entire operating frequency band.

In the work by [17], an energy harvesting antenna supporting dual-band operation for LoRaWAN and EGSM-900 networks was developed. The E-shaped antenna underwent optimization using the GWO algorithm and HFSS, resulting in dual-band functionality at 865.1 MHz and 935.8 MHz. However, drawbacks include suboptimal gain, measuring 1.0201 dB at 866 MHz and -5.4037 dB at 937 MHz. Furthermore, the lack of reconfigurability of the antenna impacts its adaptability to different operational frequencies within the LoRa spectrum.

In the study presented by [18], a dual-band PIFA antenna was designed to cater to the frequencies of 868 MHz (European LoRaWAN, ZigBee, Sigfox, and Z-Wave) and 2.4 GHz (ZigBee, Wi-Fi, Bluetooth). The antenna, implemented on an FR-4 substrate with a distinctive ground plane placement, demonstrated effective dual-band performance. However, its relatively larger dimensions measuring 100 $\times$ 40 x 1.6 mm^3 might limit its application in scenarios with space constraints. Despite optimizing impedance matching and achieving a commendable maximum gain of 4.2 dBi at 2.4 GHz, the antenna's lack of reconfigurability for other LoRa frequencies restricts its versatility across various IoT applications.

In [19], a triangular-shaped multiband printed antenna for LoRaWAN applications was introduced. Designed on an FR-4 substrate, the antenna exhibited significant dimensions, measuring 160 mm x 170 mm x 1.6 mm. Despite showcasing dual-band functionality at 400 MHz and 900.2 MHz, it achieved a maximum gain of -5.2 dB. The antenna's considerable size, limited gain, and fixed-frequency operation may pose challenges, particularly in applications where compactness, higher gain, and frequency adaptability are critical requirements.

In [20], a unique LoRa antenna designed for 868 MHz operation in both overwater and underwater surface communication scenarios was presented on an FR-4 substrate. To address bandwidth degradation issues in aquatic environments, the authors introduced a barrier (hollow) around the antenna filled with oil-impregnated papers. The resulting buffered antenna achieved an expansive bandwidth of 400 MHz, spanning from 668 MHz to 1068 MHz. Performance evaluations revealed that the sensor node with the buffered antenna could communicate up to 6 meters underwater and extended to 160 meters over the water surface. In contrast, the sensor node without the buffered antenna achieved a communication range of only 80 meters over the water surface. However, the braided antenna's dimensions, measuring 120 mm x 70 mm x 2.4 mm, may be considered relatively large, and its operation limited to a single frequency may pose constraints in applications where compactness and frequency adaptability are essential.

In a work presented by [21], a rectangular MPA for LoRaWAN applications was designed on a PCB fabricated with FR-4 material. The antenna's design aimed to augment gain and efficiency by incorporating at its ground plane two slots (T-shaped). Despite achieving a gain of 2.194 dB, which signifies improved performance, notable limitations include the antenna's non-reconfigurable nature and relatively large dimensions measuring 210.82 mm x 164.79 mm x 5.5 mm. These factors may pose challenges in scenarios where adaptability and compact size are essential considerations.

In [22], two LoRa antennas operating at 868 MHz were ingeniously designed to resemble the logos of the University of Information Technology (UIT) and Universite Cote d'Azur (UCA). The antennas were designed on an FR-4 substrate with dimensions of 34 $\times$ 80 $\times$ 0.8 mm^3. While the $S_{11} < -6$ dB characteristic suggests commendable impedance matching, a notable limitation lies in the non-reconfigurable nature of the antennas, as they operate at a fixed LoRa frequency. This lack of adaptability may restrict their versatility in applications requiring frequency adjustments or dynamic configurations.

The authors in [23] presented a dual-band antenna for LPWAN applications, covering frequencies at 433 MHz and 868 MHz. The antenna, implemented on an FR-4 substrate, exhibited modest dimensions of 90 mm x 30 mm x 1.6 mm and featured a distinctive geometric shape resembling the Universite Cote d'Azur logo. A notable drawback is the antenna's non-reconfigurable nature, limiting its adaptability to different LoRa operational frequencies. Additionally, the functionally achieved maximum gains at 433 MHz (-4.1 dB) and 868 MHz (-2.2 dB) suggest relatively low gain values in comparison to other antenna designs.

In the study by [24], an IoT terminal with dimensions (300 mm x 30 mm x 0.8 mm) was introduced, featuring three antennas designed for operation across four frequency bands. The terminal integrated antennas for dual-band GSS (Galileo L1 and L2 frequencies), and LoRa antennas at 2.4 GHz and 868 MHz. Despite the versatility of the antenna system in the IoT terminal, allowing for communication across multiple frequency bands, a notable limitation is its non-reconfigurable nature. Furthermore, while the terminal supports multiple bands, it covers only one LoRa band, specifically 868 MHz, potentially restricting its adaptability to different LoRa frequencies.

In [25], a reconfigurable antenna was developed to support multiple frequency bands, including 868 MHz for LoRaWAN and 401 MHz/466 MHz for UHF satellite communication. The antenna features meandered lines on its patch loaded with lumped components, and its resonance frequency is controlled by a PIN diode. In the in-active mode, the antenna operates at 466 MHz, while in the ON state, it operates at 401 MHz and 868 MHz. Despite its versatility in frequency operation, a limitation is the relatively low gain, with maximum gains of -8.5 dB, -5.2 dB, and -2.5 dB at 401 MHz, 466 MHz, and 868 MHz, respectively.

In [26], a dual-band wearable patch antenna designed for BLE-2.4 GHz and LoRa 868 MHz applications was introduced. The antenna utilizes silver-ink-printed polystyrene fabrics for the radiator and ground plane, with a neoprene substrate. Employing an aperture-coupled feeding technique, the antenna achieves dual-band functionality without a conventional metallic SMA connector, enhancing its suitability for wearables. Despite large dimension of 150 mm^2, the antenna is non-reconfigurable and covers only the 868 MHz frequency for LoRa, limiting its adaptability to different LoRa bands.

In [27], an MPA with a double leaf-shaped structure was hosted on an FR-4 substrate, featuring dimensions of $22 \times 34\ mm^2$. Covering all sub 1-GHz LoRa bands, including 433 MHz, 915 MHz, and 868 MHz, the antenna suits diverse LoRa applications. While boasting a gain of 2.56 dB for efficient signal transmission and reception, its wideband nature makes it susceptible to interference, particularly due to the proximity of frequencies like 868/915 MHz.

Recent investigations [28], [29] present LoRa antennas with triple band frequency reconfigurable features. The antenna employs a PIN diode mechanism to facilitate frequency selection among 868 MHz, 433 MHz and 915 MHz, providing adaptability for diverse LoRa bands. With dimensions less than that of a standard credit card (80 mm $\times$ 50 mm). They have attained up to 2 dBi peak gain. Despite their capability for frequency reconfiguration, the relatively large sizes of the antennas need to be reduced further for their suitability for very compact IoT solutions.

This paper introduces an innovative and compact monopole antenna with dual-band frequency reconfigurability (868/915 MHz) for LoRa applications, featuring a compact design of 40 $\times$ 42 x 1.6 mm^3. Unlike many designs suffering from limitations such as single-frequency operation, large profiles, lack of reconfigurability, and low gain, this antenna addresses these concerns. It utilizes machine learning for resonance frequency prediction, a novel approach not explored in the reviewed literature. Notably, the majority of prior works rely solely on full-wave simulation software without considering ML-based optimization. The study critically observes that previous designs often lack comprehensive evaluation, specifically in real-world conditions using a LoRa system. Unlike most, [23] is an exception, but it does not assess the RSSI using the LoRa system. An experimental setup was used to meticulously evaluate RSSI of the proposed antenna, a crucial metric for wireless communication quality, in an open environment—a football field at Universiti Teknologi PETRONAS, minimizing interference and reflecting surfaces. This comprehensive approach enhances the understanding and practical applicability of the presented antenna.

The paper unfolds as follows: Section II details the antenna's design and structure, while Section III explores its frequency-switching techniques. In Section IV, a comprehensive parametric study using CST MWS is conducted. Section V investigates antenna's optimization using machine learning. Findings and analysis are presented in Section VI. Sections VII-IX cover experimental validation and RSSI evaluation. The paper concludes in Section X with key insights and conclusions.

II. DESIGN AND GEOMETRY OF THE ANTENNA

Here, the proposed antenna's design and structure for operation within the 868 and 915 MHz LoRa frequency bands are presented. The primary goal is to seamlessly switch between 868 MHz and 915 MHz frequencies, facilitated by a single RF PIN Diode (BAR50-02V) from Infineon. Regulatory requirements dictate the global categorization of LoRa operating frequencies, with 868 MHz commonly utilized in Europe and 915 MHz in the United States and some Asian countries. The antenna's geometry, illustrated in Fig. 1, integrates patches of meandered monopoles on an FR-4 substrate's upper surface, 1.6 mm thick, featuring $\tan\delta = 0.02$, and $\varepsilon_r = 4.4$. Complementing this design is a partial ground positioned on the substrate's lower side as depicted in Fig. 1(b). The meandered monopoles, strategically folded based on equations in [30], facilitate resonance at 868 MHz and 915 MHz, contingent on the diode's mode. Chosen for its wide availability and cost-effectiveness, the substrate undergoes design, tuning, and analysis through CST MWS. Excitation is achieved via a 50 Ω microstrip feed line having a width of 3 mm.

A matching stub with dimensions of 18 mm $\times$ 2 mm, illustrated in Fig. 1(a), is integrated to enhance the antenna's matching at the operational bands. This stub is crucial for ensuring efficient power transfer between the antenna and the transmission line, optimizing signal transmission and reception. The inclusion of a matching stub further refines the antenna's performance, ensuring effectiveness in diverse applications within the designated frequency bands.

III. FREQUENCY SWITCHING TECHNIQUES

There is a growing interest in reconfigurable antennas due to their ability to overcome design limitations and adapt to the evolving needs of wireless communication. Researchers commonly employ various radiofrequency (RF) switches such as FET switches, PIN diodes, and MEMS switches to enable reconfiguration of antenna. The fundamental principle underlying these switches is their capacity to regulate the flow of RF current, allowing for antenna reconfigurability. Precise positioning and optimization of the RF switch are

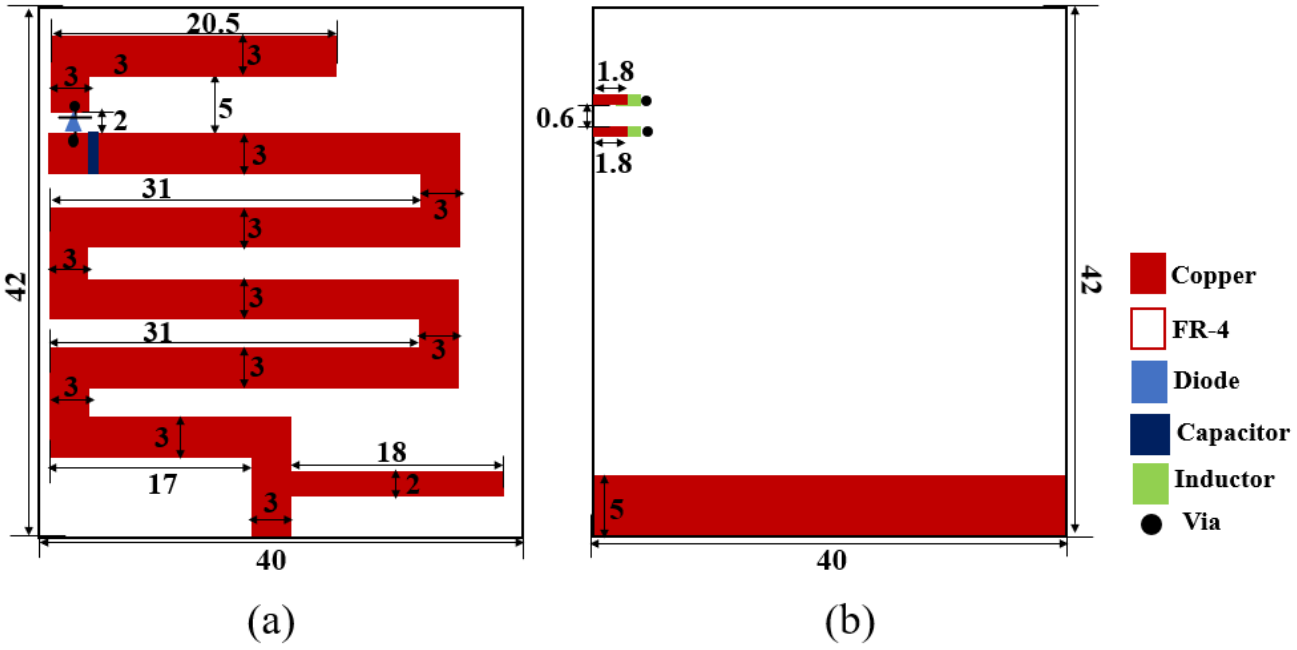

FIGURE 1. Geometry of the proposed antenna (a) Front (b) Back.

crucial aspects of effective antenna design. Among the different methods for achieving reconfigurable frequency antennas, PIN diodes are favored for their impressive handling capabilities and cost-effectiveness.

This study utilizes a single PIN diode (BAR50-02V) from Infineon to enable seamless operation of the antenna at two distinct LoRa frequencies: 868/915 MHz. The BAR50-02V, known for its low forward resistance and minimal harmonic distortions, plays a key role in facilitating swift and efficient frequency switching. In the ON state of the diode, current flows, inducing resonance at 868 MHz, while the OFF state strategically isolates specific monopole elements, generating resonance at the higher frequency of 915 MHz. This approach aligns with theoretical considerations, where the relationship between patch length and resonance is critical. The circuit representation of the PIN diode in both states depicted in Fig. 2, characterized by RLC (Resistance, Inductance and Capitance), is derived from the data sheets of the RF PIN diode.

In Fig. 2(a), during the active mode, the PIN diode exhibits a series arrangement comprising an inductor (L) and a resistor (R). The L and R are chosen to be small enough that the diode functions as a short circuit, enabling current flow within the radiating elements of the antenna. Conversely, in the OFF mode illustrated by Fig. 2(b), the diode assumes the form of a parallel combination of a capacitor (C) and a resistor (R) connected in series with an inductor (L). Specifically chosen values for these components ensure that the current flow through the radiating monopoles is impeded. The biasing circuit of the PIN diode, as depicted in Fig. 3, provides a practical understanding of the frequency-switching mechanism. The use of CST with touchstone files

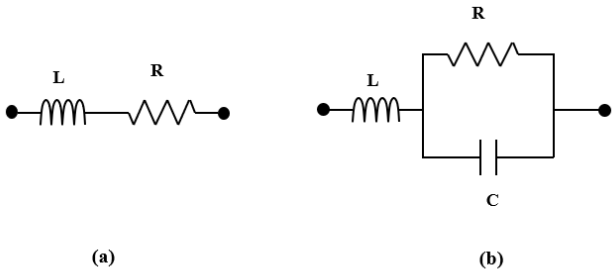

FIGURE 2. Representation of the active and in-active modes of RF PIN diode.

allows for a comprehensive insight into the S-parameters at both ON and OFF states, enhancing an understanding of this intricate frequency-switching process. Fig. 4 illustrates the plots of simulated S_{11} corresponding to the active and in-active modes of the diode. In the active mode, a resonance at 868 MHz was achieved by the antenna, the simulated S_{11} exhibits a magnitude of -19.1 dB. Conversely, in the OFF state, where the antenna operates at 915 MHz, the simulated S_{11} magnitude is 19 dB.

IV. PARAMETRIC STUDIES USING CST MWS

An extensive exploration of the antenna design's parameters was undertaken to optimize its performance. Critical parameters such as substrate length (L_s), substrate width (W_s), matching stub width (W_{mstub}), matching stub length (L_{mstub}), and ground plane length (L_g) were methodically examined to understand their effects on the designed antenna. The overarching goal of these investigations is to utilize CST MWS for identifying optimal values for these parameters,

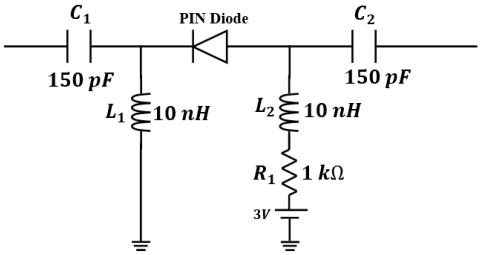

FIGURE 3. RF PIN diode biasing circuit.

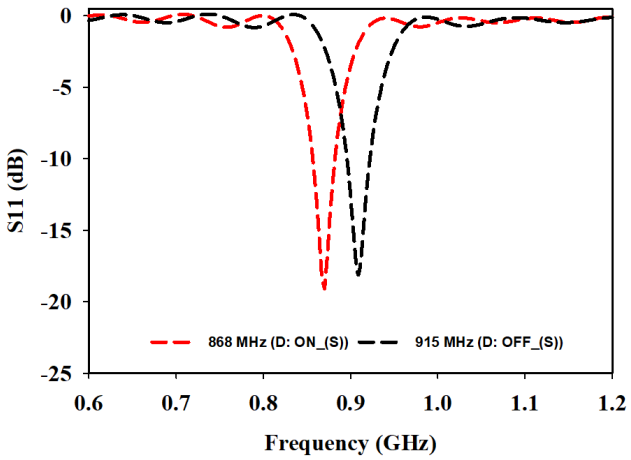

FIGURE 4. S_{11} at active and in-active modes of the PIN diode.

aiming for enhanced S_{11} characteristics and impeccable matching at the designated operating frequencies of 868 MHz and 915 MHz.

A. SUBSTRATE LENGTH (L_S) AND SUBSTRATE WIDTH (W_S)

A systematic investigation of both L_s and W_s was carried out to enhance the antenna's performance within the operational frequencies of the antenna as illustrated in Fig. 5 and Fig. 6. Fig. 5 depicts the parameter sweep conducted on L_s, ranging from 40 mm to 45 mm, with the optimal value determined as 42 mm, ensuring precise resonance and maximizing efficiency within the designated frequency bands. Similarly, Fig. 6 showcases the parameter sweep for W_s, spanning from 37 mm to 41 mm, and identifies the optimum width as 40 mm. This specific width played a crucial role in fine-tuning the antenna's response, ensuring accurate frequency operation, and enhancing overall performance. Through the optimization of both L_s and W_s, the antenna's performance was enhanced, guaranteeing optimal resonance and excellent matching at both 915 MHz and 868 MHz. This precise tuning solidifies the antenna's efficiency and reliability.

B. LENGTH OF GROUND PLANE (L_G)

Fig. 7 illustrates the optimization carried out on the ground plane length (L_g), ranging from 2 mm to 7 mm. The analysis

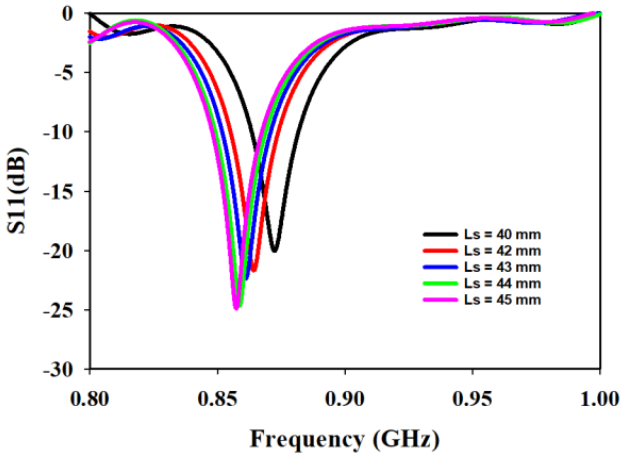

FIGURE 5. Variation of L_s and its effect on S_{11}.

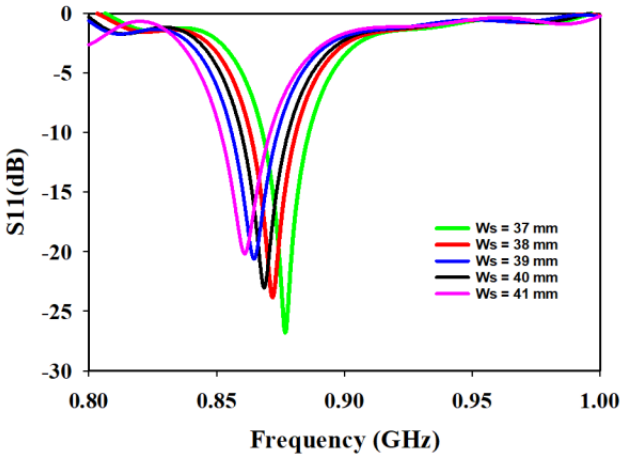

FIGURE 6. Variation of W_s and its effect on S_{11}.

revealed that an L_g of 5 mm achieved the desired resonance. This specific length played a crucial role in establishing the necessary grounding, significantly contributing to the antenna's stability and resonance characteristics.

C. LENGTH AND WIDTH OF MATCHING STUB

Parametric investigations were extended to include L_{mstub} and W_{mstub}. Fig. 8 and Fig. 9 depict the systematic exploration of L_{mstub} (ranging from 16 mm to 20 mm) and W_{mstub} (ranging from 1 mm to 4 mm), respectively. The analysis identified optimal values of 18 mm for L_{mstub} and 2 mm for W_{mstub}, resulting in the desired resonance. These dimensions played a crucial role in precisely tuning impedance matching, facilitating efficient power transfer, and minimizing signal losses.

V. MACHINE LEARNING (ML) BASED OPTIMIZATION

In this section, ML techniques, particularly regression models, are explored for predicting the resonance frequency based on antenna parameters. Conventional antenna modeling

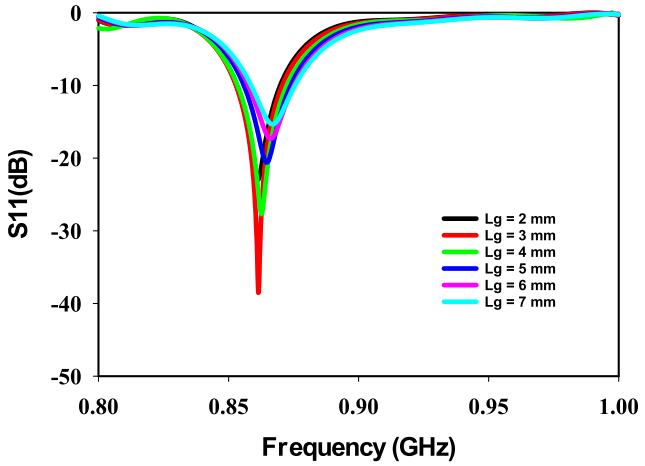

FIGURE 7. Variation of L_g and its effect on S_{11}.

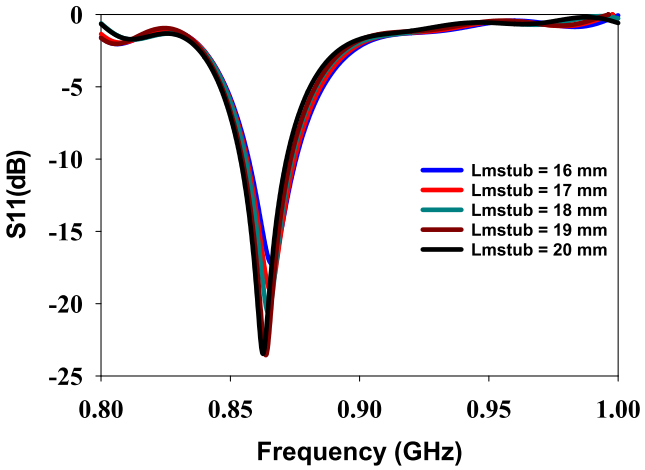

FIGURE 8. Variation of L_{mstub} and its effect on S_{11}.

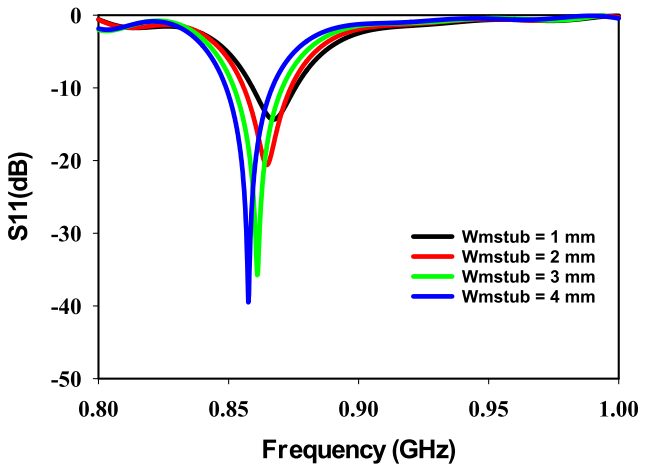

FIGURE 9. Variation of W_{mstub} and its effect on S_{11}.

often employs Commercial Computational Electromagnetics (CEM) software such as FEKO, HFSS, ADS, IE3D, and CST for obtaining solutions to partial differential equations

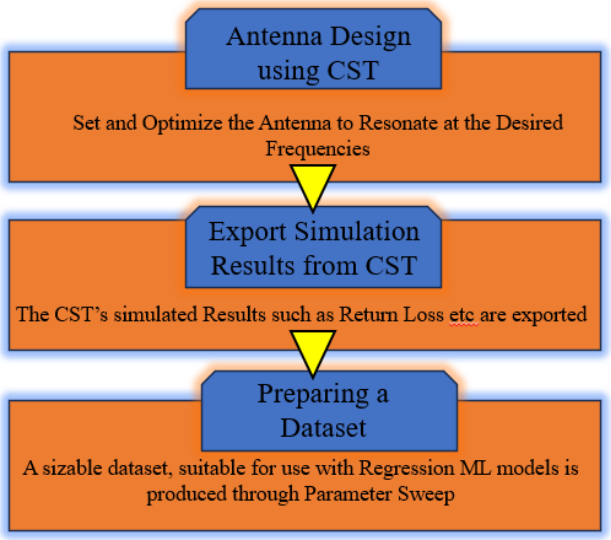

FIGURE 10. Workflow for data acquisition using ML.

under specified boundary conditions through computer-based methods. These software tools are extensively utilized for antenna design, applying Maxwell's equations to simulate the interaction between electromagnetic fields and antennas [31].

While widely applied in antenna simulation and testing [32], numerical analysis approaches like Methods of Moments (MoM), Finite Element Method (FEM), and Finite Difference Time Domain (FDTD) exhibit commonality. However, the time required for execution increases significantly in software such as CST and HFSS as the complexity of the antenna's topology grows. This limitation complicates current optimization methods, which are crucial for ensuring an antenna emits at its maximum capacity [33].

Recognizing these challenges, researchers are exploring ways to improve the effectiveness of antenna design using ML algorithms [34], [35]. The utilization of ML algorithms, with their significant speed-up capabilities while maintaining high accuracy, holds enormous potential in predicting antenna behavior and optimizing design. The success of antenna design with machine learning systems relies on the quantity, quality, and accessibility of data. Gathering sufficient data can be challenging, especially as standard antenna datasets are limited. To address this, datasets using CEM simulation software are generated from the proposed antenna across a wide range of values.

In this work, the optimization process involves two distinct stages. In the first stage, the dual-band frequency reconfigurable antenna for LoRa applications is designed in CST MWS, a simulation tool. The necessary dataset are then extracted through a parametric sweep. The flowchart outlining this process is depicted in Fig. 10. Subsequently, a machine learning model is trained on the dataset to determine the most reliable approach for predicting the resonance frequency.

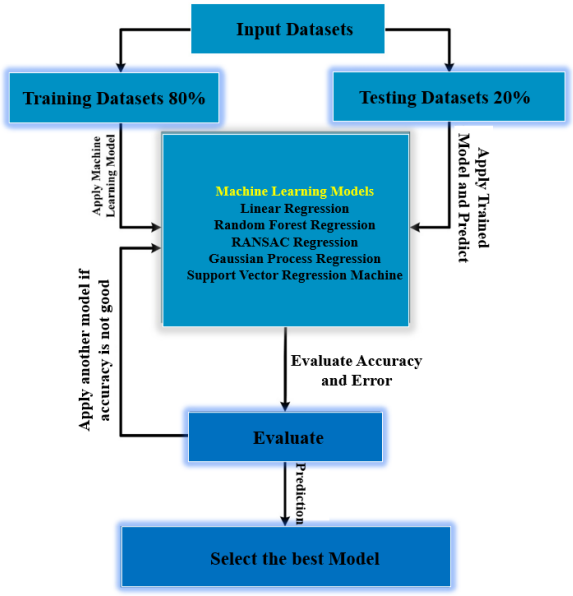

FIGURE 11. Step for developing ML algorithm.

The proposed antenna is simulated using CST MWS, generating a dataset of 164 data points. Multiple regression ML methods are employed to predict the resonance frequency. Of the total data points, 80% are utilized for the learning phase, while the remaining 20% are reserved for assessment. The dataset includes input variables such as the substrate's length, width, and height, along with the feed's width and length, matching stub length, and width. The primary output parameter is the resonance frequency, as illustrated in Fig. 11.

The machine learning technique applied to the training of the dataset considers both features and labels. Once the model training and validation are completed, the trained model can reliably predict outputs, such as resonance frequency, based on the respective inputs.

In this study, predictions are conducted using five distinct machine-learning algorithms, including Random Forest Regression, Linear Regression, RANSAC Regression, SVRM, and Gaussian Process Regression. These models are selected for their efficacy in the analysis of non-linear regression, which aligns with the study's objective of numerical predictions. The choice of regression models is particularly apt for the nature of the predictions sought. The term ''error'' serves as the primary statistic in regression analysis, measuring the variance between predicted and actual values.

All machine learning experiments are conducted in the Python simulation environment provided by Google and Google Colab. The regression models are efficiently constructed using the sci-kit learn machine learning framework. Throughout the research, including data analysis and visualization, Matplotlib is extensively utilized, ensuring a comprehensive and visually informative exploration of the results [36].

A. SELECTION OF ML MODEL

The optimal performance of a machine learning model is often achieved through the careful selection of various models. In this study, regression analysis is employed, a statistical technique designed to evaluate the cause-and-effect relationship between variables. While our problem is tackled using regression analysis, we further enhance our approach by incorporating five highly practical machine learning regression models, each briefly outlined below:

1) **Random Sampling and Consensus (RANSAC) Regression:**
RANSAC is a regression technique employed to fit models to data that may contain outliers or noise. It proves to be a robust and reliable statistical tool, particularly effective when dealing with datasets where certain observations deviate from the expected pattern or model [37].
2) **Linear Regression:**
Linear regression establishes a correlation between dependent and independent variables through a linear model, indicating that alterations in independent variables align proportionally with dependent factors. This model presupposes that errors, signifying discrepancies between anticipated and actual values, adhere to a normal distribution and display consistent variance. The fundamental aim of linear regression is to depict the association between two variables by aligning a linear equation with observed data. In this context, the initial variable acts as an explanatory factor, while the second functions as the dependent variable [38].
3) **Random Forest Regression:**
Random Forest, an ensemble methodology, effectively deals with both classification and regression challenges. By merging the Bootstrap and Aggregation technique, widely known as bagging, with multiple decision trees, this strategy entails training diverse models using randomly chosen subsets of the data [35]. Random Forest Regression proves invaluable, demonstrating proficiency in managing high-dimensional data and capturing intricate non-linear relationships between features and the target variable [39].
4) **Support Vector Regression:**
Support Vector Regression (SVR) stands as a crucial element within Statistical Learning Theory, acclaimed for its efficacy in modeling time-sequential events. Introduced by Vapnik, the Support Vector Machine (SVM) leans on the Vapnik–Chervonenkis Dimension theory and the principle of structural risk minimization. SVM offers distinctive advantages in addressing challenges of pattern recognition marked by nonlinearity and high dimensionality, especially in scenarios with a limited number of samples. Its intrinsic resistance to the curse of dimensionality ensures superior generalization through structural risk minimization, mitigating overfitting and necessitating fewer training features [40].

The global and unique solution provided by SVM, framed as a convex optimization problem, contributes to its robustness, simplicity in geometric interpretation, and sparse solution [41].

5) **Gaussian Process Regression (GPR):** Gaussian Process Regression is a preferred non-parametric method for machine learning in regression tasks. Unlike standard regression models that assume specific functional forms for relationships between variables, GPR offers a flexible framework, making minimal assumptions about the underlying data distribution. It excels in assessing uncertainty and modeling intricate, non-linear interactions. GPR is known as a supervised machine learning technique that successfully addresses regression and classification issues, providing advantages such as effective performance with small datasets and the provision of uncertainty metrics for predictions [38]. Essentially, GPR operates as nonparametric kernel-based probabilistic models, offering a general-purpose solution for supervised learning in regression and probabilistic classification [42], [43].

B. METRICS FOR PERFORMANCE MEASUREMENT

The primary measure of success in regression analysis is the level of error. To assess the relative performance of each method, various statistical indicators were employed. A battery of five statistics was used to evaluate the algorithms' performance, and the results were compared. The evaluation metrics included root-mean-square error (RMSE), coefficient of determination (R^2), variance score, and mean absolute error (MAE).

Mean Absolute Error (MAE) is a statistic utilized to gauge the disparity between predicted values and actual values in a regression problem. A lower MAE indicates higher accuracy in predicting the dependent variable. Equation (1) illustrates the formulation of MAE [44].

$$\mathrm{MAE} = \frac{1}{n}\sum_{i=1}^{n}|P_i - O_i| \tag{1}$$

where, n is the number of errors, $|P_i - O_i|$ represents the absolute error.

The widely used representation of the regression loss function is the Mean Squared Error (MSE). This loss is computed by averaging the squared differences between the observed and predicted values across all data points. The formulation for MSE is given by (2).

$$\mathrm{MSE} = \frac{1}{N}\sum_{i=1}^{N}(y_i - \hat{y}_i)^2 \tag{2}$$

A frequently employed statistic to assess the accuracy of a prediction model, particularly within the domain of regression analysis, is the Root Mean Squared Error (RMSE). This metric obtained from (3) gauges the typical magnitude of differences, referred to as errors or residuals, between predicted and observed values within a dataset.

$$RMSE = \sqrt{\frac{1}{n}\sum_{i=1}^{n}(P_i - O_i)^2} \tag{3}$$

The coefficient of determination (R^2) given by (4) for a regression model expresses the amount of variation in the dependent variable (the variable you're attempting to forecast) that can be attributed to changes in the model's independent (predictive) variables. Another way of stating this is to measure how well the model's independent variables adequately explain the dependent variable. R-squared is commonly used to determine how well a regression model fits the data.

If the coefficient of determination (R^2) is zero, it signifies that the model's independent variables do not account for any of the variance in the dependent variable, indicating no predictive value in the model. Conversely, an R^2 value of 1 means that all the variability in the dependent variable is perfectly explained by the model. Achieving a perfect R-squared of 1 is rare in practice and generally indicates overfitting.

$$R^2 = 1 - \frac{\sum_{i=1}^{N}(y_i - \hat{y}_i)^2}{\sum_{i=1}^{N}(y_i - \bar{y})^2} \tag{4}$$

The R-squared (R^2) value, often termed the "variance score" given by (5) in machine learning and regression studies, serves as a statistical indicator. It quantifies the proportion of total variance in the dependent variable that can be ascribed to the independent variables of the model. Essentially, it elucidates the extent to which the model captures the variation in the dependent variable and its alignment with the dataset.

$$\text{explained variance}(y, \hat{y}) = 1 - \frac{\mathrm{Var}(y - \hat{y})}{\mathrm{Var}(y)} \tag{5}$$

C. RESULTS AND ANALYSIS OF ML BASED PREDICTION

The comparison of five regression models in predicting resonant frequency based on six input parameters is summarized in Table 1. The accuracy of each algorithm is assessed using MAE, MSE, and RMSE metrics, resulting in scores of 6.39%, 1.38%, and 6.98%, respectively. Gaussian Process Regression stands out with remarkable performance, achieving an R-squared score of 92.87% and a variance score of 93.77%. Fig. 12 visually presents the comparison of outcomes obtained from the various models.

The values of the predicted and simulated resonance frequencies, along with their differences, are displayed in Table 2. In this study, there are 32 samples that make up the test set, representing 20% of the entire dataset. The variability in the difference between simulated and predicted resonance frequencies is illustrated in Fig. 13. The GPR model was chosen due to its superior accuracy in predicting frequencies compared to other ML models considered.

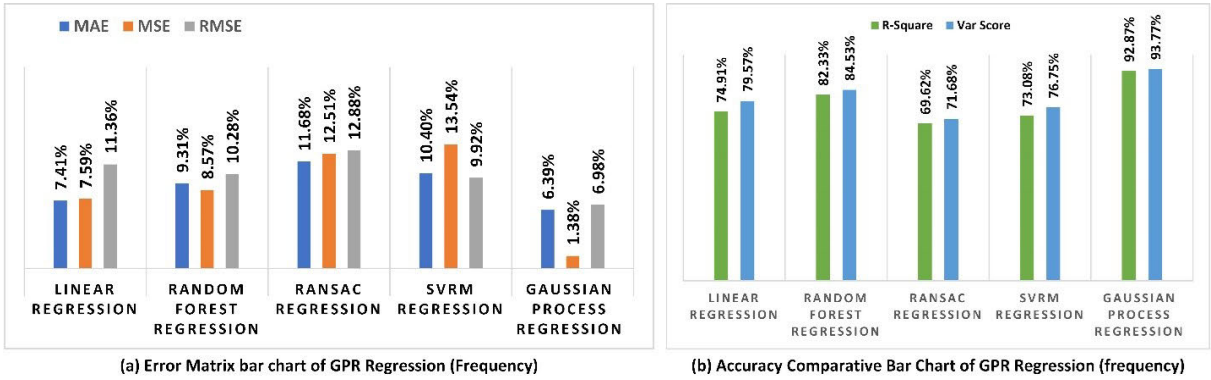

(a) Error Matrix bar chart of GPR Regression (Frequency)

(b) Accuracy Comparative Bar Chart of GPR Regression (frequency)

FIGURE 12. Comparison of regression models.

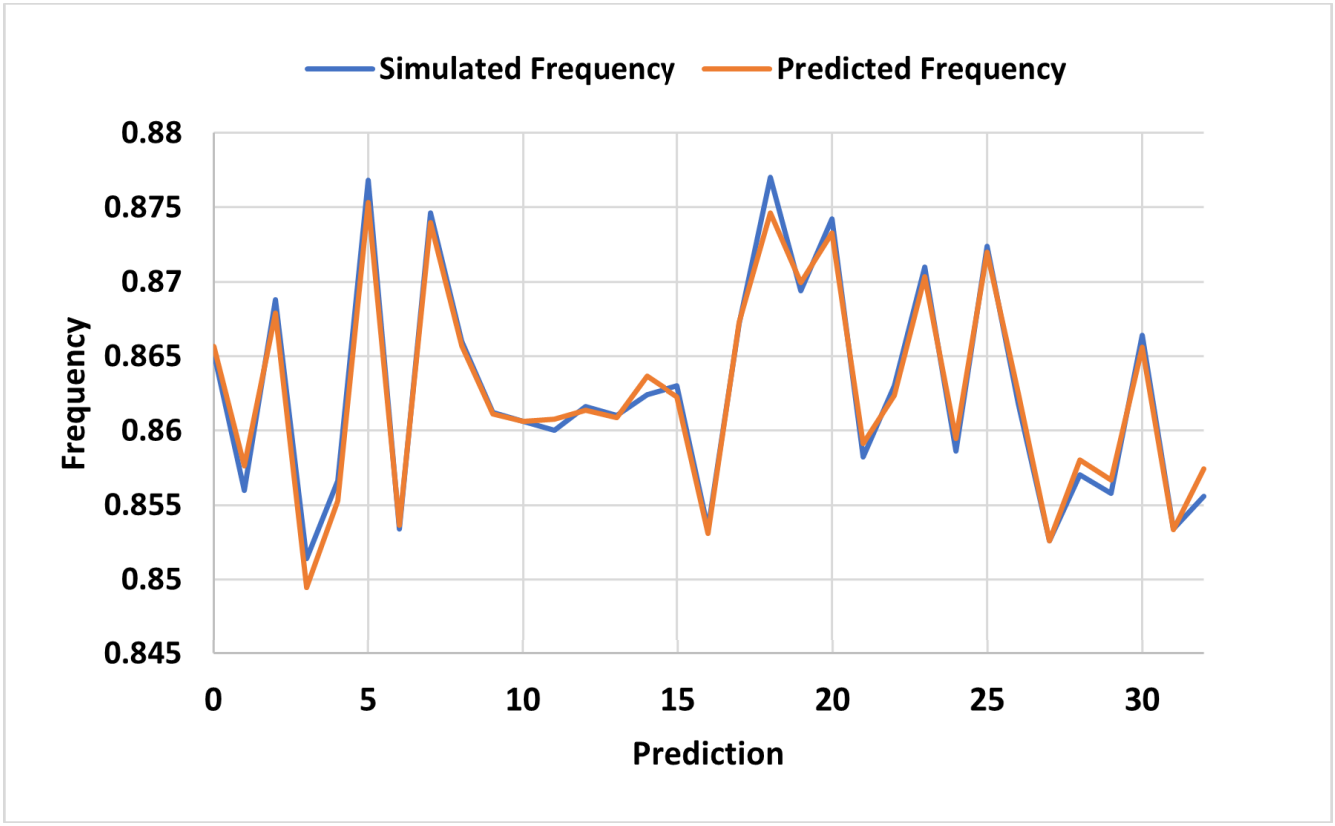

FIGURE 13. Comparison between simulated and predicted frequencies using GPR regression.

VI. RESULTS AND ANALYSIS

An in-depth analysis of the proposed antenna's performance is presented, focusing on critical metrics such as return loss (S_{11}), surface current distribution, radiation patterns, gain, and efficiency. A thorough comparison between simulation and measurement results is carried out across these parameters. The fabrication of the proposed antenna prototype, depicted in Fig. 14, takes place on a cost-effective FR-4 substrate. To ensure accuracy and reliability, measurements of the (S_{11}), radiation pattern, and gain of the proposed antenna were conducted.

A. RETURN LOSS

The S_{11} (measured and simulated) responses of the antenna in both active and in-active modes of the PIN diode are illustrated in Fig. 15 and Fig. 16. The antenna exhibits operation at 868 MHz and 915 MHz, depending on the mode of the diode. In the ON state, the antenna functions at 868 MHz with magnitudes of −19.1 dB (simulation) and −20.5 dB (measurement). This behavior is attributed to the forward-biased diode allowing RF signals through all the meandered antenna's monopole elements. Conversely, in the OFF state, the antenna resonates at 915 MHz, with

TABLE 1. Comparison of performance of various prediction models.

Algorithms	MAE	MSE	RMSE	R-Square	Var Score
Linear Regression	7.41%	7.59%	11.36%	74.91%	79.57%
Random Forest Regression	9.31%	8.57%	10.28%	82.33%	84.53%
RANSAC Regression	11.68%	12.51%	12.88%	69.62%	71.68%
SVRM Regression	10.40%	13.54%	9.92%	73.08%	76.75%
Gaussian Process Regression	6.39%	1.38%	6.98%	92.87%	93.77%

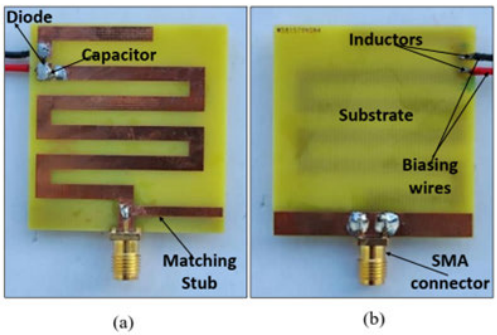

FIGURE 14. Prototype of the proposed antenna (a) Front (b) Back.

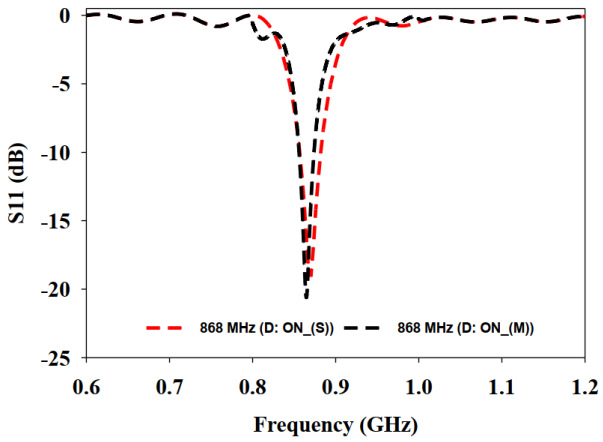

FIGURE 15. Comparison of (S_{11}) when the PIN diode is ON (868 MHz).

magnitudes of −19 dB (simulation) and −16 dB (measurement), as a consequence of the diode being in reverse bias, isolating the uppermost monopoles. In both cases, the measured and simulated S_{11} exhibit agreement. Remarkably, the proposed antenna spans two significant LoRa bands (915 MHz and 868 MHz), establishing it as a novel antenna with these characteristics. The antenna demonstrates good matching in each scenario, with comparatively good matching.

B. SURFACE CURRENT DISTRIBUTION ANALYSIS

The performance of an antenna is closely connected with how electric current flows within its radiating elements. This fundamental aspect enables precise control over antenna

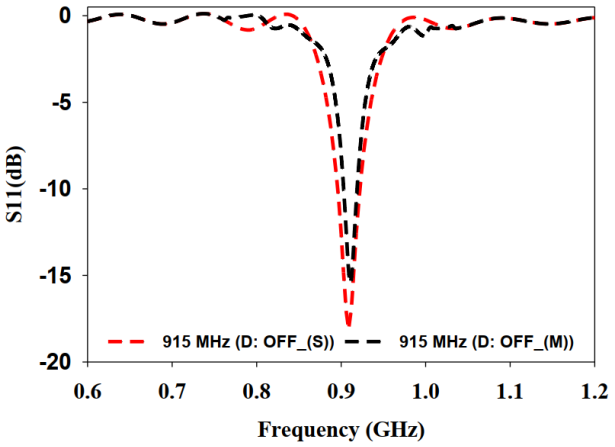

FIGURE 16. Comparison of (S_{11}) when the PIN diode is OFF (915 MHz).

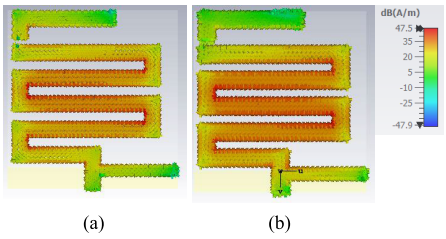

FIGURE 17. Current distribution (a) Active Mode (868 MHz) (b) In-active Mode (915 MHz).

behavior, allowing for resonance at specific frequencies for particular applications. In this study, a comprehensive examination to explore the behavior of the monopole elements that constitute the proposed antenna is conducted. Each of these elements is fundamental to establishing resonance under different diode states. The analysis uncovered distinct monopoles responsible for generating resonance at different frequencies. Notably, these elements exhibited maximum surface current density precisely at their respective resonance frequencies, a pivotal factor influencing the manifestation of resonance phenomena.

The surface current distribution in the ON/OFF states of the diodes is vividly depicted in Fig. 17. In Fig. 17(a), the current distribution during the ON state is showcased. The illustration reveals a harmonious convergence of all antenna elements, establishing resonance at 868 MHz. This convergence is facilitated by the unobstructed flow of electric current across all monopole elements, thanks to the forward biasing of the diode. The biasing enables seamless current flow, synchronizing the behavior of the elements and resulting in the observed resonance at 868 MHz.

In contrast, Fig. 17(b) depicts a distinctive behavior when the diode is in the OFF state. The current flow is selectively constrained from entering the uppermost inverted L-shaped monopole of the antenna. This constraint leads to resonance at 915 MHz due to the shortened electrical length of the antenna caused by the restricted current flow.

TABLE 2. Comparison between simulated and predicted resonant frequencies utilizing GPR.

No.	Frequency (Simulated)	Frequency (Predicted)	No.	Frequency (Simulated)	Frequency (Predicted)
1	0.8652	0.865658	17	0.8672	0.867291
2	0.856	0.857645	18	0.877	0.874629
3	0.8688	0.867889	19	0.8694	0.869911
4	0.8514	0.849459	20	0.8742	0.873281
5	0.8566	0.855298	21	0.8582	0.859128
6	0.8768	0.875303	22	0.863	0.862343
7	0.8534	0.853657	23	0.871	0.87031
8	0.8746	0.873955	24	0.8586	0.859462
9	0.866	0.865694	25	0.8724	0.871977
10	0.8612	0.861107	26	0.8618	0.862498
11	0.8606	0.860612	27	0.8526	0.852598
12	0.86	0.86077	28	0.857	0.858034
13	0.8616	0.861354	29	0.8558	0.856679
14	0.861	0.860859	30	0.8664	0.865574
15	0.8624	0.863641	31	0.8534	0.853349
16	0.863	0.86224	32	0.8556	0.857397

C. ANALYSIS OF RADIATION PATTERNS

Here, the proposed antenna's radiation characteristics are explored to understand its coverage and communication effectiveness within the LoRa frequency bands. Fig. 18 and Fig. 19 provides a clear visualization of the antenna's patterns in both the diodes's active and in-active modes, offering valuable insights into its directional properties.

At 868 MHz, corresponding to the ON state of the diode, Fig. 18 illustrates bidirectional and omnidirectional radiation characteristics for the E-plane and H-plane respectively. These patterns are crucial for LoRa communications, allowing the antenna to effectively cover a broad area while directing communication efforts in specific directions.

Conversely, in the OFF state of the diode operating at 915 MHz, Fig. 19 shows that the antenna maintains bidirectional and omnidirectional radiation characteristics for the E-plane and H-plane respectively.

Notably, these patterns closely resemble those observed during the ON state of the diode. This consistency highlights the antenna's stable characteristics across different operational states, emphasizing its reliability and predictability in diverse communication scenarios. These distinctive radiation characteristics underscore the proposed antenna's flexibility and adaptability at both 868 MHz and 915 MHz, making it a robust choice for LoRa IoT applications.

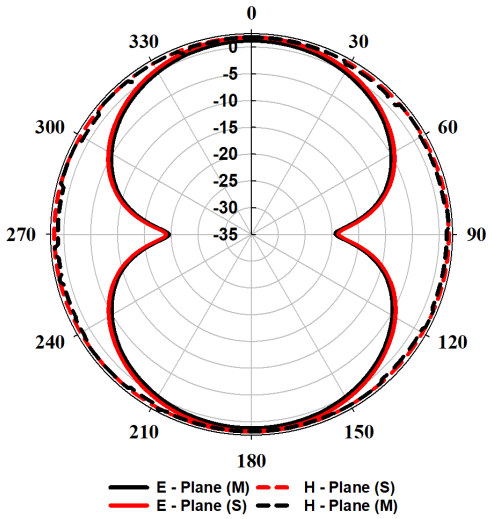

FIGURE 18. Radiation patterns for active mode (868 MHz).

D. GAIN AND EFFICIENCY

This section investigates the efficiency and gain characteristics of the proposed antenna. In the active mode of the switch, the antenna exhibits a gain of 1.9 dBi at 868 MHz, which slightly increases to 2 dBi at 915 MHz. Additionally, the antenna maintains an efficiency consistently above 70% at both frequencies. Fig. 20 visually represents plots of the gain and efficiency as functions of frequency, offering a comprehensive overview of the antenna's performance.

The efficiency and gain metrics are particularly relevant in antenna design. The peak gain of 2 dBi at 915 MHz emphasizes the antenna's capability to focus signals in specific directions, making it suitable for applications such as LoRa IoT.

Additionally, the antenna's effectiveness in converting input power into radiated energy is evident, with measured efficiency closer to 70% at both bands. In LoRa IoT applications, where energy conservation is crucial for extending device battery life, high efficiency becomes paramount. The proposed antenna's efficiency ensures that a significant portion of the input power contributes to communication, minimizing energy wastage and maximizing the overall efficiency of the network.

Table 3 provides a comprehensive comparison between the performance of the proposed antenna and established counterparts, emphasizing its exceptional superiority. The antenna's key strength is its compact design, dual-band coverage, and reconfigurable features specifically for the LoRa frequency bands at 868 and 915 MHz. Notably, it has attained a maximum gain of 2 dBi, rendering it highly suitable

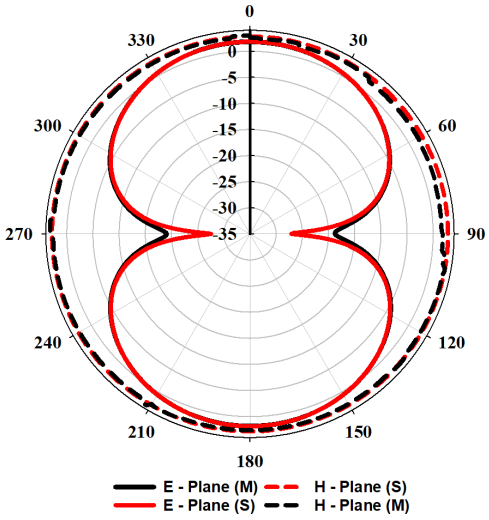

FIGURE 19. Radiation patterns for in-active mode (915 MHz).

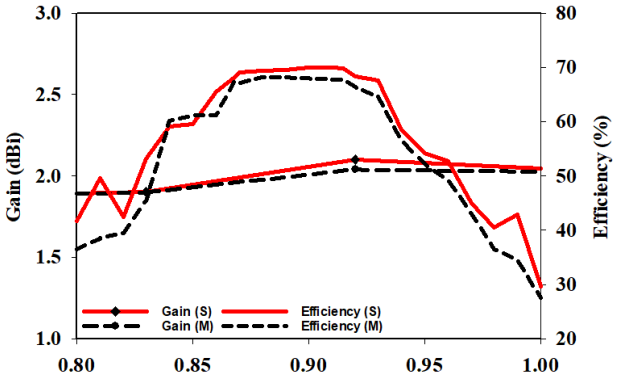

FIGURE 20. Plots of gain and efficiency as functions of frequency for the ON and OFF state of the diode.

for LoRa communication applications. Taken together, these distinctive features underscore the antenna's outstanding performance in comparison to alternatives documented in the current literature.

VII. EXPERIMENTAL VALIDATION

This section provides a detailed overview of the methodology employed to assess the proposed antenna's capability in enhancing the Received Signal Strength Indicator (RSSI) within a LoRa system. RSSI is a crucial metric that measures the signal strength received by the antenna, offering insights into the quality and reliability of wireless communication. It quantifies the power level of the received signal, indicating the signal's robustness against interference and distance attenuation. A higher RSSI value signifies a stronger and more reliable signal, essential for effective data transmission and reception in wireless communication systems.

RSSI plays a pivotal role in evaluating antenna efficiency, particularly in scenarios where maintaining a stable and strong connection is crucial, such as in long-range IoT applications facilitated by LoRa technology. A comprehensive understanding of RSSI dynamics enables the evaluation of antenna performance under varying conditions, assisting in the selection of optimal configurations for specific applications.

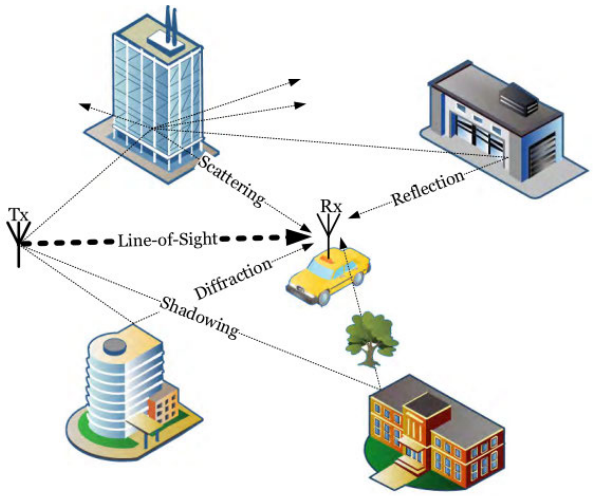

FIGURE 21. Components of received radio frequency signal.

The received signal can be viewed as a function of frequency and antenna properties, with distance playing a predominant role (6):

$$P_r = f(d, f, A_p) \tag{6}$$

where P_r is the power of the received signal,

d represents the separation distance between the Rx and Tx,

f is frequency of operation, and

A_p represents antenna characteristics

The received signal comprises various components, illustrated in Fig. 21, where the Line-of-Sight (LOS) component stands out as the most robust [45].

The Received Signal Strength Indicator (RSSI) can be modeled as follows (7):

$$P_r = D + \psi + \alpha \tag{7}$$

- D represents the deterministic part of the signal, influenced by path-loss models like the single-slope model, Stanford University Interim (SUI) Model, Hata model, Okumura's Model, etc. It is mainly governed by the Line-of-Sight (LOS) component.
- ψ represents large-scale fading or shadowing, characterized as a random variable that predicts signal variation in obstructed environments.
- α signifies small-scale fading or multipath effects, resulting from reflected, scattered, diffracted, and attenuated signal copies reaching the receiver. [45].

As highlighted in Section I, antennas designed for LoRa have not been thoroughly evaluated in outdoor/indoor settings

TABLE 3. Performance comparison of the proposed antenna with existing work.

Ref.	Year	Bands	Freq (MHz)	Substrate	Patch material	Gain (dBi)	Reconfigurable?	All LoRa Freq?	Size (mm^2)
[13]	2018	1	402.4-441.6	FR-4 (NA)	Copper	-6	NO	YES	125 x 20
[15]	2020	4	865-880 1525-1605 1790-1868 2085-2125	FR-4 (4.4)	Copper	1.29 3.94 1.15 0.89	NO	NO	82.8 x 44.85
[19]	2021	2	400 900.2	FR-4 (NA)	Copper	-5	NO	YES	160 x 170
[20]	2021	1	868	FR-4 (4.3)	Copper	2.11	NO	YES	120 x 70
This work	**2023**	**2**	**868** **915**	FR-4 (4.4)	**Copper**	**1.9** **2**	**YES**	**YES**	**42 x 40**

FIGURE 22. Site of experiment.

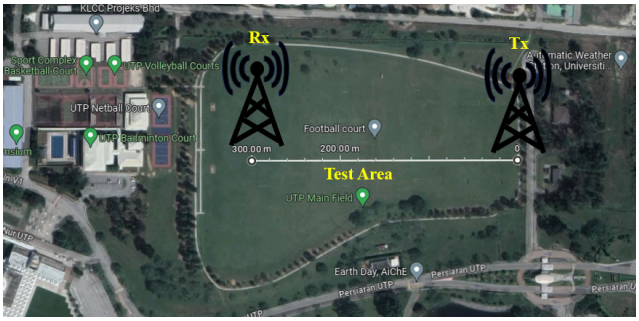

FIGURE 23. Positioning of Tx and Rx.

for RSSI. This aspect adds a novel dimension to the present study, addressing a gap in the existing literature.

VIII. EXPERIMENTAL SETUP

The experimental environment as shown in Fig. 22 was carefully chosen to replicate real-world scenarios, utilizing an open football field at Universiti Teknologi PETRONAS, Malaysia. This deliberate selection aimed to minimize interference from surrounding structures and surfaces, ensuring the experiments closely resembled practical applications for accurate and relevant outcomes.

A. SETUP AND DEVICES

LoRa communication modules, consisting of both transmitting (Tx) and receiving (Rx) devices, were meticulously prepared as shown in Fig. 23. These devices incorporated LoRa SX1276 wireless communication modules based on TTGO LoRa32 technology, equipped with antennas operating at a frequency of 915 MHz.

Two types of antennas were employed: the proposed Dual-Band Frequency Reconfigurable Antenna and a conventional monopole whip antenna. The validation process encompassed four configurations, involving both antennas as Tx and Rx individually, allowing for a comprehensive assessment.

The devices as shown in Fig. 24 were initialized, configured for the operating frequency of 915 MHz. Systematic experiments involved moving the Tx away from the Rx in precise 50 m intervals. Data packets were transmitted and RSSI values were recorded, providing insights into signal strength and quality.

The transmitter's relocation to subsequent positions facilitated a thorough assessment of signal strength at distances up to 300 m. The recorded RSSI values were meticulously analyzed, enabling a detailed comparison between the proposed antenna and the conventional monopole whip antenna. Graphical visualizations conveyed the differences in signal strength between the two antennas.

IX. PROPOSED ANTENNA'S RSSI EVALUATION

A comprehensive bidirectional performance assessment was conducted by employing the proposed antenna on both the Tx and Rx modules concurrently, contrasting with a scenario where the conventional antenna was utilized for both modules. This experimental configuration allowed for an independent evaluation of each antenna's performance in both transmission and reception modes.

The RSSI values were measured and analyzed for both scenarios, providing distinct insights into each antenna's performance when handling the dual responsibility of

FIGURE 24. Setup of Tx and Rx.

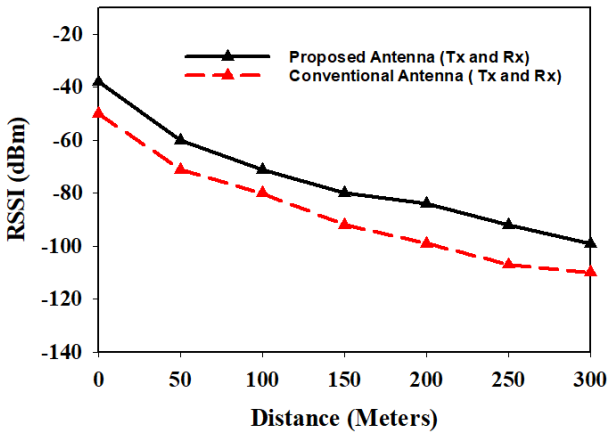

FIGURE 25. Comparison of RSSI.

transmission and reception in a real-world communication setting. Fig. 25 illustrates the RSSI plots for the two distinct cases. The analysis demonstrates a notable improvement in signal strength when using the proposed antenna compared to the conventional antenna across distances up to 300 m.

The proposed antenna as depicted by Fig. 25 consistently outperformed its conventional counterpart at each measurement point. This proved its efficacy in enhancing signal reception. At the 300 m mark, the RSSI for the proposed antenna registers at -99 dBm, while the conventional

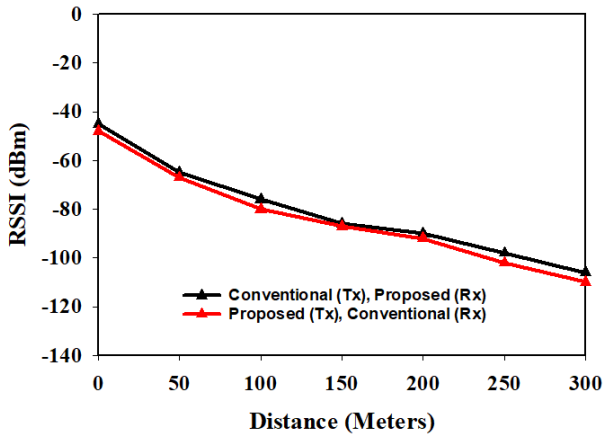

FIGURE 26. RSSI of the reciprocity test.

antenna lags behind at -110 dBm. This substantial difference underscores the superior signal strength achieved by the proposed antenna, positioning it as a compelling choice for reliable communication over long distances.

A. RECIPROCITY TEST AND ANALYSIS

To confirm the reciprocity between the proposed antenna and the conventional antenna, we conducted additional tests by swapping the antennas between the Rx and Tx modules. In Case 1, the conventional antenna was used on the Rx module, while the proposed antenna was used for the Tx module. Conversely, in Case 2, we switched the antennas, with the proposed antenna used on the Rx antenna and the conventional antenna as the Tx antenna. The obtained RSSI values for both cases were plotted and are presented in Fig. 26.

The reciprocity tests reveal a noteworthy observation: the RSSI values measured for a distance up to 300 m for Case 1 precisely align with those obtained in Case 2, as illustrated in Fig. 26. This consistency in RSSI values between the two cases indicates the presence of reciprocity, demonstrating that the proposed antenna's performance characteristics remain consistent whether used for transmission or reception. The agreement in RSSI values reinforces the reliability and symmetry in the behavior of the proposed antenna in both Tx and Rx configurations.

Reciprocity is a crucial aspect in wireless communication systems, ensuring that the antenna's performance remains consistent regardless of its role in transmission or reception. The results of these reciprocity tests underscore the robustness of the proposed antenna design, affirming its suitability for bidirectional communication applications where symmetry and reliability are paramount.

The comparison of RSSI results between the conventional antenna and the proposed antenna, as well as with results from previous literature, provides valuable insights into the performance of the antennas in the context of LoRa communication. The RSSI values, measured at various

TABLE 4. Comparison of RSSI values for different antennas.

Ref.	LoRa Technology	RSSI (dBm)						Frequency (MHz)
		D = 50 m	100 m	150 m	200 m	250 m	300 m	
[46]	LoRa SX1276	-86	NA	NA	-95	NA	NA	915
[47]	Semtech SX1272	-82	NA	NA	-108	NA	-115	915
Conventional Whip Antenna	LoRa SX1276	-71	-80	-92	-99	-107	-110	915
Proposed Antenna	**LoRa SX1276**	**-60**	**-71**	**-80**	**-84**	**-92**	**-99**	**915**

distances from 50m to 300m, serve as a quantitative measure of signal strength, influencing the reliability and range of communication.

Firstly, when comparing the proposed antenna with the conventional whip antenna, it is evident that the proposed antenna consistently outperforms the conventional antenna across all distances. At 300m, the RSSI for the proposed antenna is -99 dBm, whereas the conventional antenna lags behind at -110 dBm. This consistent improvement in RSSI values highlights the superior signal reception capabilities of the proposed antenna.

Secondly, comparing the results with previous literature, particularly [46] and [47] as presented in Table 4, showcases the competitive performance of the proposed antenna. In the 300m scenario, the RSSI for the proposed antenna (-99 dBm) surpasses the RSSI values reported in the literature for the same distance. This suggests that the proposed antenna excels in maintaining signal strength over extended distances compared to the referenced LoRa technologies.

The improvement in RSSI values exhibited by the proposed antenna is crucial for ensuring dependable communication, particularly in scenarios where establishing a strong and consistent connection is essential. This contrast emphasizes the effectiveness of the proposed antenna in enhancing signal reception within a LoRa communication system, positioning it as a promising solution for applications with extended-range requirements.

The comparison of RSSI results confirms the superiority of the proposed antenna over the conventional counterpart and demonstrates its competitive performance when compared to established LoRa technologies outlined in previous literature. This affirms the antenna's effectiveness in practical scenarios and underscores its potential for applications that demand robust and long-range communication capabilities.

X. CONCLUSION

This paper presents a novel and compact monopole antenna with dual-band frequency reconfigurability specifically designed for applications in LoRa IoT, representing a notable advancement in wireless communication technology. Operating at 868 MHz and 915 MHz, aligning with LoRa bands across major continents, this antenna bridges a crucial gap in the current landscape, as there is currently no existing compact reconfigurable antenna designed for these specific LoRa bands within the ISM bands below 1 GHz.

Constructed on an accessible FR-4 substrate, the antenna leverages meandered monopole patches to achieve a compact size of 40×42 mm^2 ($0.12\,\lambda_0 \times 0.12\,\lambda_0$), with λ_0 representing the wavelength in free space corresponding to 868 MHz. The implementation of a single RF PIN diode enables seamless switching between 868 MHz and 915 MHz bands. The design, simulation, and optimization processes were meticulously executed using CST MWS software.

The incorporation of supervised regression machine learning (ML) models, particularly Gaussian Process Regression, for predicting resonance frequencies at different antenna parameters demonstrated exceptional accuracy, achieving an impressive R-squared score of 92.87% and a variance score of 93.77%. This underscores the efficacy of Gaussian Process Regression as the preferred choice for resonance frequency prediction. This approach saved computational time for the full-wave simulation software (CST MWS), contributing to a more streamlined design process.

Experimental validation in a real-world setting encompassed open-field testing of the fabricated prototype antenna in a football field at Universiti Teknologi PETRONAS, Malaysia. The assessment of the antenna's performance on a LoRa transceiver system based on LoRa SX1276 demonstrated consistent superiority. The Received Signal Strength Indicator (RSSI) of the proposed antenna consistently outperformed the conventional antenna by an average of -12 dBm at each point within a range of up to 300 m, affirming its enhanced signal reception capabilities.

The presented antenna is a promising solution for wireless sensor nodes in long-range applications, substantiated by its robust performance metrics and meticulously conducted experimental validations.

ACKNOWLEDGMENT

The authors would like to thank the Centre of Graduate Studies, Universiti Teknologi PETRONAS, Malaysia, and the Petroleum Technology Development Fund (PTDF) for their invaluable support in providing access to state-of-the-art research facilities that has been instrumental in the successful execution of this study.

REFERENCES

[1] M. Jouhari, N. Saeed, M.-S. Alouini, and E. M. Amhoud, "A survey on scalable LoRaWAN for massive IoT: Recent advances, potentials, and challenges," *IEEE Commun. Surveys Tuts.*, vol. 25, no. 3, pp. 1841–1876, 3rd Quart., 2023, doi: 10.1109/COMST.2023.3274934.

[2] A. Ikpehai, B. Adebisi, K. M. Rabie, K. Anoh, R. E. Ande, M. Hammoudeh, H. Gacanin, and U. M. Mbanaso, "Low-power wide area network technologies for Internet-of-Things: A comparative review," *IEEE Internet Things J.*, vol. 6, no. 2, pp. 2225–2240, Apr. 2019.

[3] P. Asghari, A. M. Rahmani, and H. H. S. Javadi, "Internet of Things applications: A systematic review," *Comput. Netw.*, vol. 148, pp. 241–261, Jan. 2019.

[4] S. F. Hassan, A. Mahmood, S. A. Hassan, and M. Gidlund, "Wireless mediation for multi-hop networks in time critical industrial applications," in *Proc. IEEE Globecom Workshops (GC Wkshps)*, Dec. 2018, pp. 1–6.

[5] S. Lee, J. Lee, H.-S. Park, and J. K. Choi, "A novel fair and scalable relay control scheme for Internet of Things in LoRa-based low-power wide-area networks," *IEEE Internet Things J.*, vol. 8, no. 7, pp. 5985–6001, Apr. 2021.

[6] S. Bagwari, A. Gehlot, R. Singh, N. Priyadarshi, and B. Khan, "Low-cost sensor-based and LoRaWAN opportunities for landslide monitoring systems on IoT platform: A review," *IEEE Access*, vol. 10, pp. 7107–7127, 2022.

[7] J. M. Marais, R. Malekian, and A. M. Abu-Mahfouz, "LoRa and LoRaWAN testbeds: A review," in *Proc. IEEE AFRICON*, Sep. 2017, pp. 1496–1501.

[8] M. S. Yahya, S. A. B. Hamzah, K. N. Ramli, F. C. Seman, M. Abu, S. Nordin, N. N. N. A. Malik, and M. S. Mustapa, "Multiband and wideband characteristics of grid array antenna," *AIP Conf. Proc.*, vol. 2564, no. 1, 2023, Art. no. 070003.

[9] M. S. Yahya, S. Soeung, F. E. Chinda, C. Sovuthy, N. B. M. Nor, S. K. A. Rahim, and U. Musa, "A compact dual band microstrip patch antenna for LoRa IoT applications," in *Proc. IEEE Int. RF Microw. Conf. (RFM)*, Dec. 2022, pp. 1–4.

[10] M. Sani Yahya and S. K. A. Rahim, "15 GHz grid array antenna for 5G mobile communications system," *Microw. Opt. Technol. Lett.*, vol. 58, no. 12, pp. 2977–2980, Dec. 2016.

[11] P. P. Singh, P. K. Goswami, S. K. Sharma, and G. Goswami, "Frequency reconfigurable multiband antenna for IoT applications in WLAN, Wi-Max, and C-band," *Prog. Electromagn. Res. C*, vol. 102, pp. 149–162, 2020.

[12] W. Wanpare, A. Paisal, and S. Chalermwisutkul, "A compact 923 MHz monopole antenna for LoRaWAN IoT applications," in *Proc. Int. Conf. Power, Energy Innov. (ICPEI)*, Oct. 2020, pp. 53–56.

[13] Q. Zhang and Y. Gao, "Embedded antenna design on LoRa radio for IoT applications," in *Proc. 12th Eur. Conf. Antennas Propag.*, London, U.K., 2018, p. 3. [Online]. Available: https://digital-library.theiet.org/content/conferences/10.1049/cp.2018.0920

[14] A. Pandey and M. V. D. Nair, "Inset fed miniaturized antenna with defected ground plane for LoRa applications," *Proc. Comput. Sci.*, vol. 171, pp. 2115–2120, Jan. 2020.

[15] A. D. Boursianis, M. S. Papadopoulou, J. Pierezan, V. C. Mariani, L. S. Coelho, P. Sarigiannidis, S. Koulouridis, and S. K. Goudos, "Multiband patch antenna design using nature-inspired optimization method," *IEEE Open J. Antennas Propag.*, vol. 2, pp. 151–162, 2021.

[16] M. Tarbouch, "A compact PIFA antenna for Internet Of Things network LORAWAN at 900 MHz band," 2019. [Online]. Available: https://api.semanticscholar.org/CorpusID:203688571

[17] A. D. Boursianis, S. K. Goudos, T. V. Yioultsis, and K. Siakavara, "Low-cost dual-band E-shaped patch antenna for energy harvesting applications using grey wolf optimizer," in *Proc. 13th Eur. Conf. Antennas Propag. (EuCAP)*, Mar. 2019, pp. 1–5.

[18] A. Reha, M. Tarbouch, and A. E. Amri, "A dual band compact PIFA antenna for Internet of Things networks Sigfox, LoRaWAN and Zigbee," in *Proc. Colloque Objets Systèmes Connectés*, Mar. 2019, pp. 1–5.

[19] M. V. Krishna and G. S. N. Raju, "Triangle shaped antenna design for IoT-based LoRaWAN applications," *SAMRIDDHI, J. Phys. Sci., Eng. Technol.*, vol. 13, no. 1, pp. 8–11, Jun. 2021.

[20] A. Dala and T. Arslan, "Design, implementation, and measurement procedure of underwater and water surface antenna for LoRa communication," *Sensors*, vol. 21, no. 4, p. 1337, Feb. 2021.

[21] A. Mushtaq, S. H. Gupta, and A. Rajawat, "Design and performance analysis of LoRa LPWAN antenna for IoT applications," in *Proc. 7th Int. Conf. Signal Process. Integr. Netw. (SPIN)*, Feb. 2020, pp. 1153–1156.

[22] L. H. Trinh, T. Q. K. Nguyen, D. D. Phan, V. Q. Tran, V. X. Bui, N. V. Truong, and F. Ferrero, "Miniature antenna for IoT devices using LoRa technology," in *Proc. Int. Conf. Adv. Technol. Commun. (ATC)*, Oct. 2017, pp. 170–173.

[23] F. Ferrero and M. B. Toure, "Dual-band LoRa antenna: Design and experiments," in *Proc. IEEE Conf. Antenna Meas. Appl. (CAMA)*, Oct. 2019, pp. 243–246.

[24] Y. Wang, L. Santamaria, F. Ferrero, and L. Lizzi, "Design of a multi-antenna portable IoT terminal," in *Proc. IEEE Conf. Antenna Meas. Appl. (CAMA)*, Nov. 2021, pp. 597–599.

[25] A. Bouyedda, B. Barelaud, and L. Gineste, "Design and realization of an UHF frequency reconfigurable antenna for hybrid connectivity LPWAN and LEO satellite networks," *Sensors*, vol. 21, no. 16, p. 5466, Aug. 2021.

[26] N. F. Ibrahim, P. A. Dzabletey, H. Kim, and J.-Y. Chung, "An all-textile dual-band antenna for BLE and LoRa wireless communications," *Electronics*, vol. 10, no. 23, p. 2967, Nov. 2021.

[27] R. Roges, P. K. Malik, and S. Sharma, "A compact wideband antenna with DGS for IoT applications using LoRa technology," in *Proc. 10th Int. Conf. Emerg. Trends Eng. Technol.-Signal Inf. Process.*, Apr. 2022, pp. 1–4.

[28] M. S. Yahya, S. Soeung, N. S. S. Singh, Z. Yunusa, F. E. Chinda, S. K. A. Rahim, U. Musa, N. B. M. Nor, C. Sovuthy, and G. E. M. Abro, "Triple-band reconfigurable monopole antenna for long-range IoT applications," *Sensors*, vol. 23, no. 12, p. 5359, Jun. 2023.

[29] M. S. Yahya, S. Soeung, F. Emmanuel Chinda, S. K. B. A. Rahim, U. Musa, N. B. M. Nor, and S. Cheab, "A compact reconfigurable multi-frequency patch antenna for LoRa IoT applications," *Prog. Electromagn. Res. M*, vol. 116, pp. 77–89, 2023.

[30] H. H. M. Ghouz, M. F. A. Sree, and M. A. Ibrahim, "Novel wideband microstrip monopole antenna designs for WiFi/LTE/WiMax devices," *IEEE Access*, vol. 8, pp. 9532–9539, 2020.

[31] C.-C. Chen and J. L. Volakis, Eds., "Ultra-wide bandwidth antenna design," in *Antenna Engineering Handbook*, 4th ed. New York, NY, USA: McGraw-Hill, 2007, ch. 19.

[32] W. C. Gibson, *The Method of Moments in Electromagnetics*. Boca Raton, FL, USA: CRC Press, 2021.

[33] N. Sarker, P. Podder, M. R. H. Mondal, S. S. Shafin, and J. Kamruzzaman, "Applications of machine learning and deep learning in antenna design, optimization, and selection: A review," *IEEE Access*, vol. 11, pp. 103890–103915, 2023.

[34] M. A. Haque, N. Sarker, N. S. Sawaran Singh, M. A. Rahman, M. N. Hasan, M. Islam, M. A. Zakariya, L. C. Paul, A. H. Sharker, G. E. M. Abro, M. Hannan, and R. Pk, "Dual band antenna design and prediction of resonance frequency using machine learning approaches," *Appl. Sci.*, vol. 12, no. 20, p. 10505, Oct. 2022.

[35] H. M. E. Misilmani, T. Naous, and S. K. A. Khatib, "A review on the design and optimization of antennas using machine learning algorithms and techniques," *Int. J. RF Microw. Comput.-Aided Eng.*, vol. 30, no. 10, pp. 1–28, Oct. 2020.

[36] M. A. Haque, D. Saha, S. S. Al-Bawri, L. C. Paul, M. A. Rahman, F. Alshanketi, A. Alhazmi, A. H. Rambe, M. A. Zakariya, and S. S. B. Hashwan, "Machine learning-based technique for resonance and directivity prediction of UMTS LTE band quasi Yagi antenna," *Heliyon*, vol. 9, no. 9, Sep. 2023, Art. no. e19548.

[37] R. Subbarao and P. Meer, "Beyond RANSAC: User independent robust regression," in *Proc. Conf. Comput. Vis. Pattern Recognit. Workshop*, Jul. 2006, p. 101.

[38] J. Manasa, R. Gupta, and N. S. Narahari, "Machine learning based predicting house prices using regression techniques," in *Proc. 2nd Int. Conf. Innov. Mech. Ind. Appl. (ICIMIA)*, Mar. 2020, pp. 624–630.

[39] N. M. Sai, M. S. Saravanan, and P. Subramanian, "A novel framework of network packet loss detection using random forest algorithm over support vector machine learning algorithms to improve accuracy," in *Proc. Int. Conf. Knowl. Eng. Commun. Syst. (ICKES)*, Dec. 2022, pp. 1–4.

[40] E. Yoshino, F. I. Kurniadi, and B. Juarto, "Forecasting rice production in Indonesia using regression techniques: A comparative analysis of support vector machine, linear regression, and XGBoost regression," in *Proc. 10th Int. Conf. ICT Smart Soc. (ICISS)*, Sep. 2023, pp. 1–5.

[41] D. Wang, J. Peng, Q. Yu, Y. Chen, and H. Yu, "Support vector machine algorithm for automatically identifying depositional microfacies using well logs," *Sustainability*, vol. 11, no. 7, p. 1919, Mar. 2019.

[42] Y. Sui and L. Zhang, "Visual tracking via locally structured Gaussian process regression," *IEEE Signal Process. Lett.*, vol. 22, no. 9, pp. 1331–1335, Sep. 2015.

[43] D. Xiao, L. Guo, W. Liu, and M. Hou, "Improved Gaussian process regression inspired by physical optics for the conducting target's RCS prediction," *IEEE Antennas Wireless Propag. Lett.*, vol. 19, no. 12, pp. 2403–2407, Dec. 2020.

[44] E. M. S. El-Said, M. Abd Elaziz, and A. H. Elsheikh, "Machine learning algorithms for improving the prediction of air injection effect on the thermohydraulic performance of shell and tube heat exchanger," *Appl. Thermal Eng.*, vol. 185, Feb. 2021, Art. no. 116471.

[45] H. Kwasme and S. Ekin, "RSSI-based localization using LoRaWAN technology," *IEEE Access*, vol. 7, pp. 99856–99866, 2019.

[46] A. Vazquez-Rodas, F. Astudillo-Salinas, C. Sanchez, B. Arpi, and L. I. Minchala, "Experimental evaluation of RSSI-based positioning system with low-cost LoRa devices," *Ad Hoc Netw.*, vol. 105, Aug. 2020, Art. no. 102168.

[47] M. Anjum, M. A. Khan, S. A. Hassan, A. Mahmood, H. K. Qureshi, and M. Gidlund, "RSSI fingerprinting-based localization using machine learning in LoRa networks," *IEEE Internet Things Mag.*, vol. 3, no. 4, pp. 53–59, Dec. 2020.

MUHAMMAD S. YAHYA (Graduate Student Member, IEEE) received the B.Eng. degree in electrical and electronics engineering from Abubakar Tafawa Balewa University, Bauchi, Nigeria, in 2010, and the M.Eng. degree in electronics and telecommunications engineering from Universiti Teknologi Malaysia, in 2016. He is currently pursuing the Ph.D. degree in electrical and electronics engineering with Universiti Teknologi PETRONAS, Malaysia. His research interests include antennas and propagation, the IoT, reconfigurable antennas, and RF/microwave circuits.

SOCHEATRA SOEUNG (Senior Member, IEEE) received the B.Eng. degree (Hons.) in electrical and electronics, major in computer system architecture from Universiti Teknologi PETRONAS, Malaysia, and the M.Sc. and Ph.D. (by Research) degrees in RF and microwave engineering from Universiti Teknologi PETRONAS, Malaysia. He was awarded and funded as a Research Officer in RF microwave engineering under several Ministry of Higher Education Malaysia and industrial funding projects during his graduate study. He was involved in designing, implementing, and testing RF subsystem components and RF communication link. Currently, he is a Lecturer and the Computation and Communication Cluster Leader of the Electrical and Electronics Engineering Department, Universiti Teknologi PETRONAS. He has been awarded with more than ten funding's from Malaysian government, industries, and university research collaborations. Over the years, he has been a Contributor of more than 35 technical research journals and conference papers. His research interests include RF microwave filter design and synthesis for multiband, multi-mode filter on planar and cavity structures, computer-aided tuning, and optimization techniques. He is currently a member of MTT and serves as a Secretary of IEEE ED/MTT/SSC Penang Chapter, Malaysia.

SHARUL KAMAL ABDUL RAHIM (Senior Member, IEEE) received the degree in electrical engineering from The University of Tennessee, Knoxville, TN, USA, the M.Sc. degree in engineering (communication engineering) from Universiti Teknologi Malaysia (UTM), and the Ph.D. degree in wireless communication system from the University of Birmingham, U.K., in 2007. After he graduated from The University of Tennessee,, Knoxville, he spent three years in the industry. After the M.Sc. degree, he joined UTM, in 2001, where he is currently a Professor with the Wireless Communication Centre. He has published over 200 learned articles in journals, including *IEEE Antenna and Propagation Magazine*, IEEE TRANSACTIONS ON ANTENNA AND PROPAGATION, and the IEEE ANTENNA AND PROPAGATION LETTERS. He also has many patents. His research interests include antenna design, smart antenna systems, beamforming networks, and microwave devices for fifth generation mobile communication. He is a Senior Member of the IEEE Malaysia Section; a member of the Institute of Engineer Malaysia; a Professional Engineer with BEM; and a member of the Eta Kappa Nu Chapter, The University of Tennessee, Knoxville, and the International Electrical Engineering Honor Society. He is currently an Executive Committee Member of the IEM Southern Branch.

UMAR MUSA (Graduate Student Member, IEEE) received the bachelor's degree in electrical engineering from Bayero University, Kano, Nigeria, in 2012, and the M.Eng. degree in electronic and telecommunication engineering from Universiti Teknologi Malaysia (UTM), Malaysia, in 2016. He is currently pursuing the Ph.D. degree with the Department of Communication Engineering, Faculty of Electrical and Electronic Engineering, Universiti Tun Hussein Onn Malaysia (UTHM). He is also a Lecturer with the Department of Electrical engineering, Bayero University, Kano. His research interests include but is not limited to, the design of RF and microwave devices and active antennas measurement. He has been a member of the Council for the Regulation of Engineering of Nigeria, since 2019.

SAEED S. BA HASHWAN received the B.Eng. degree in microelectronic engineering from the School of Microelectronic Engineering and the M.Sc. degree in nanoelectronics engineering from the Institute of Nanoelectronics Engineering, University Malaysia Perlis, in 2014 and 2017, respectively. He is currently pursuing the Ph.D. degree with the Department of Electrical and Electronic Engineering, Universiti Teknologi PETRONAS, Malaysia. His current research interests include MEMS, nanodevices, biosensors, simulation, fabrication of gas and chemical sensors, design, modeling, fabrication, and characterization of sensors and actuators, and the Internet of Things (IoT).

MD. ASHRAFUL HAQUE (Graduate Student Member, IEEE) received the B.Sc. degree in electronics and electronic engineering (EEE) from the Rajshahi University of Engineering and Technology (RUET), Bangladesh, and the M.Sc. degree from the Islamic University of Technology (IUT), Bangladesh. He is currently pursuing the Ph.D. degree with the Department of Electrical and Electronic Engineering, Universiti Teknologi PETRONAS, Malaysia, He is also on leave from Daffodil International University (DIU), Bangladesh. His research interests include microstrip patch antenna, sub 65G application, and regression model machine learning on antenna design.